Novel Jamming Mechanism for Dry Separation of Particles by Density

D. Kumar, S. M. Iveson, and K. P. Galvin

ARC Research Hub for Advanced Technologies for Australian Iron Ore, Newcastle Institute for Energy and Resources, University of Newcastle, University Drive, Callaghan, NSW 2308

Abstract

Previous work on a novel separation device called the Sink-Hole Fluidizer has been extended to investigate the effect of increasing the Sink-Hole diameter from 13 mm up to 60 mm. This device consists of a pair of mesh screens with 1 mm square apertures mounted above the surface of a vibrated fluidized bed. The upper mesh contains a large central hole referred to as a Sink-Hole. The fluidized granular media, nominally 0.2 mm sand particles, expanded up through the large Sink-Hole, spread radially and deposited across the upper mesh, and then sifted back into the lower fluidized zone. The effective density of the medium at the mouth of the Sink-Hole was determined by examining the probability of large tracer particles of a given density floating over or sinking through the Sink-Hole. It was seen previously for a 13 mm diameter Sink-Hole that the separation density exceeded the bulk density of the fluidized medium, and often also even the skeletal density of the granular media itself. Similar results were achieved here, even for a significant increase in the Sink-Hole diameter up to 60 mm. Moreover, the separation density was largely independent of the size of the tracer particles covering the range 2.8 to 8.0 mm, a sign of genuine density-based separation. The underlying mechanism was attributed to a self-organised, tenuous, jamming condition that develops at the mouth of the Sink-Hole. As the diameter of the Sink-Hole increased, the separation density decreased, while the speed at which the sorting of the test particles occurred increased significantly. A 60 mm diameter Sink-Hole achieved a steady state separation within approximately 10 seconds, and a remarkably sharp density-based separation.

Keywords: Dry separation, fluidized bed, density-based separation, iron ore, gravity separation, vibration

1.0 Introduction

In the minerals industry, the value of a particle often correlates directly with its density (Wills & Finch, 2016). Hence these particles are often characterized by the sink-float method, using a liquid medium of a specific density. If the particle floats, then its density is lower than that of the liquid, while conversely if the particle sinks its density is higher than that of the liquid. A series of liquid baths of progressively higher density are used to quantify the density distribution of the mined particles. Comparison of the feed, product and tailings streams in this manner allows the performance of large-scale gravity separation devices to be evaluated.

The buoyancy force acting on a test particle in a liquid-fluidized bed has been the subject of considerable conjecture. It is recognized that the true buoyancy force acting on a particle is fundamentally governed by the weight of the actual fluid displaced (Clift et al., 1987). In the fluidized state, the net weight force acting on the particle is balanced by the dissipative drag force arising from the fluid motion relative to the particle. Batchelor (1982) examined the problem in the limit as the particles forming the surrounding suspension become small relative to the size of the test sphere, confirming the effective buoyancy force acting on the sphere is that calculated using the average density of the medium. In this limit, the dissipative processes within the suspension produce a drag force that matches this effective weight force. Thus, fine particles can be added to a liquid to alter the effective medium density. The anecdotal evidence for particles in a gas-solid fluidized bed is similar, namely that particles segregate in an upwards direction if of lower density than the effective density of the fluidized medium.

Recently, a novel system involving a gas-solid fluidized bed referred to as the Sink-Hole fluidizer has been introduced (Kumar et al., 2018). The work was motivated by the need to achieve dry separation of particles typically between 1-10 mm under large scale industrial conditions (Dwari & Rao, 2007; Oshitani et al., 2010, 2011, 2013). The effective separation density of the medium was observed to be not only higher than the average medium density, but also higher than the skeletal density of the media particles. The result obtained was unexpected, and certainly puzzling. This paper explores the issue further, in terms of the granular state of the sand medium to propose a new mechanism to account for the elevated separation density.

Of specific interest was the effect of the Sink-Hole diameter on the separation. For the relatively small 13 mm diameter Sink-Hole used previously the kinetics of separation were relatively slow, but the separation condition robust. An industrial process demands rapid and robust separation. It was anticipated that a larger Sink-Hole would increase the kinetics, but uncertain whether the separation would remain robust and sharp. This study investigated these issues to determine the potential for improved separation, and achieve an improved understanding of the separation mechanism.

2.0 Theory

Gas-solid fluidized beds consist of granular particles (media) suspended in a gas such as air. The air is usually supplied to a plenum chamber, and then distributed evenly under pressure through the lower base of the fluidization zone via a porous distributor. At relatively low superficial fluid velocities, the air permeates through the packed granular medium, supporting in part the weight of the particles (Rhodes, 2008). At the so-called minimum fluidization velocity, U_{mf}, this dissipative drag matches sufficiently the force needed to support the buoyant weight of the particles. The system dilates slightly; the particles are then fully supported by the fluid drag, typically at a voidage of about 0.4. When the superficial velocity is increased further, there is sometimes a narrow region of uniform particulate expansion (Geldart Type A particles), but often the bed fails to expand homogeneously (Geldart Type B particles), and instead, the excess air passes through the granular medium as bubbles. Some systems with extremely fine or extremely coarse media display behaviours such as channelling or spouting respectively, but this paper is not concerned with such systems (Geldart, 1973; Kunii & Levenspiel, 1991).

Granular materials tend to exist in either a lean state, for example in fast pneumatic conveying (fast fluidization), or in a dense fluidized or packed bed state. The lean phase can be considered as gaseous in nature, the fluidized state to be liquid-like, and the packed bed to be solid-like. This strong analogue between granular mechanics and molecular dynamics has resulted in new ways of describing granular materials (Gidaspow, 1994), for example, granular temperature. The critical transition from the solid-like to liquid-like state coincides with a loss of direct solid-solid compressive strength, akin to the so-called temperature-dependent glass transition phenomenon.

The introduction of vibration to the fluidized bed can have a profound effect on the fluidization (Beeckmans & Macwilliam, 1986; Marring et al., 1994; Mawatari et al., 2001; Mori, 1990). The

vibration can vary in terms of its direction, frequency, and amplitude, while its impact can vary even further depending on the granular medium, bed geometry, bed mass, and particle weight. The vibration represents an energy source, which can cause a significant reduction in the minimum fluidization velocity. Moreover, the vibration can suppress the formation of gas bubbles within the fluidized bed. Thus, vibrated fluidization offers the opportunity for producing a uniform bed expansion in response to an increasing superficial fluidization velocity, similar to the expansion of liquid fluidized beds. Thus, the vibration provides for a further degree of freedom beyond the binary nature of conventional beds.

Dry density-based separation processes have at an industrial scale been mainly used in coal beneficiation, typically covering the particle size range from 6-50 mm (Dwari & Rao, 2007; Patil & Parekh, 2011). Below 10 mm, and especially below 6 mm, the performance of these continuous industrial separators has been reportedly poor, although improved results have been reported for batch fluidized beds (Dwari & Rao, 2007, Luo et al., 2008, Patil & Parekh, 2011). The dry separation of denser minerals such as iron ore is notably more difficult with much poorer performance. Experimental results have been reported for iron ore at a laboratory scale, achieving satisfactory results for particles larger than 20 mm in diameter, but little or no separation for particles finer than 10 mm (Oshitani et al., 2010, Oshitani et al., 2013). Table 1 shows details of some typical recent studies using air dense medium fluidized bed separators at both commercial and laboratory scale for coal and iron ore beneficiation. Systems involving relatively large particles in excess of 10 mm, and also systems involving particles of relatively low density are able to achieve satisfactory separations. However, systems involving relatively fine (< 10 mm) and/or high density particles (> 3000 kg/m^3) have largely been neglected.

Table 1: Results of some recent studies using air dense medium fluidized bed separators for coal and mineral beneficiation (D_{50} is the separation density, and Ep is the Ecart probable; see Equation 1).

Application	Feed Size (mm)	D_{50} (kg/m^3)	Ep (kg/m^3)	Remarks	Reference
Large scale continuous coal separation	6-50	1300-2200	500-700	50 t/h (operating capacity) commercial plant. Fine coal particles below 6 mm had poor separation.	Dwari & Rao, 2007
Lab scale batch separation of coal	0.5-6	1810	700	Vibrated air dense medium fluidized bed.	Luo et al., 2008
Lab scale batch separation of iron ore	>17.6	2850		Particles below 17.6 mm scatter in the bed without floating or sinking.	Oshitani et al., 2010
Lab scale continuous separation of iron ore	11.1-31.5	2850		140 kg of iron ore fed in 42 min (200 kg/h).	Oshitani et al., 2013

3.0 Materials and Methods

3.1 Equipment and Materials

This paper is concerned with the novel fluidized bed arrangement shown in Figure 1, consisting of a 200 mm diameter column, with a pair of mesh screens located at a higher elevation (Kumar et al., 2018). The mesh screens had apertures with a nominal 1 mm square pitch. In the centre of the upper mesh was a very much larger opening, which is referred to as a Sink-Hole, which was varied from 13 mm to 60 mm in diameter. The maximum Sink-Hole size used in this research was limited to 60 mm for practical reasons, as it became too difficult to insert the plug without also accidentally pushing down particles into the underflow.

The sand media was the same as that used by Kumar et al. (2018). It had a nominal particle size of 0.2 mm and its size distribution is shown in Figure 2. Its skeletal density was 2643 kg/m^3 and minimum fluidisation velocity was U_{mf} = 2.51 cm/s. The sand was fluidized with air and the air velocities are reported as the superficial velocity (volumetric flow rate divided by the cross-sectional area of the bed). The bed was vibrated at 50 Hz frequency by mounting it on a Kason vibratory device as the source of the vibration with a 90^o lead angle setting .The combination of vibration and secondary screen mesh promoted homogeneous bed expansion, as reported previously (Kumar et

al., 2018). The mass of sand used was set sufficient to ensure that once fluidizing air and vibration were turned on, the medium rose up to the level of the upper mesh screen and Sink-Hole.

Air can flow easily through both the screen mesh and the Sink-Hole. However, the sand media can flow through the Sink-Hole much more easily than through the mesh as the granular media particle size was approximately a third of the mesh aperture. This means that the flux of sand passing up through the Sink-Hole was considerably greater than through the mesh. This excess sand, after rising up through the Sink-Hole, spilled out over the surrounding mesh, dispersed across the mesh surface due to the vibration, before sifting back through the mesh. Thus, the air, which passed through the granular media and out of the system, may in fact filter marginally from the granular material on route through the Sink-Hole. The sand media developed a positive upwards velocity through the Sink-Hole, matched by a net downwards return flux through the mesh. This circulation through the Sink-Hole and mesh was superimposed over a batch fluidized bed below.

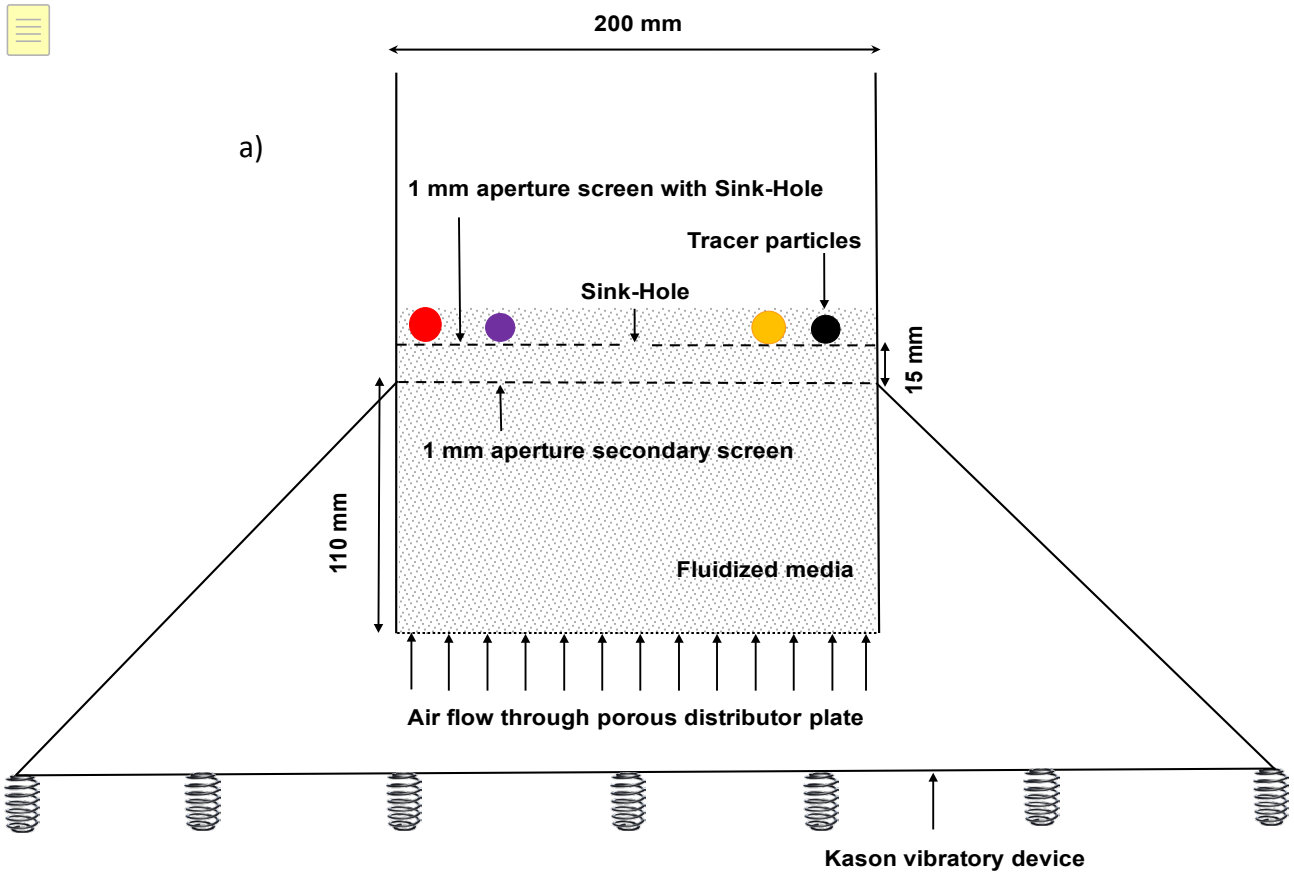

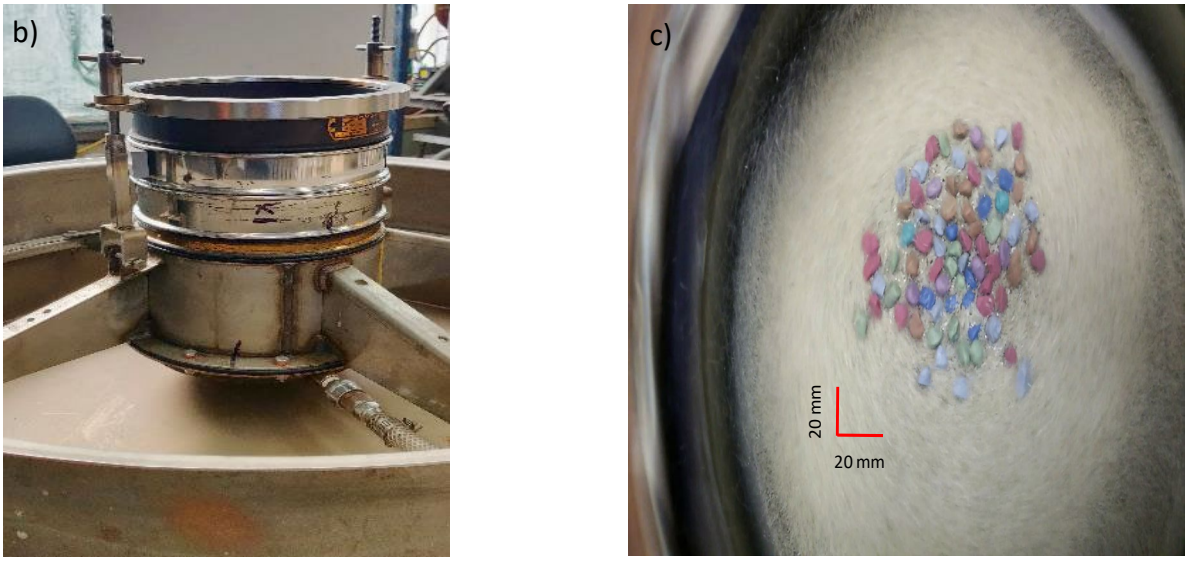

Figure 1: a) Schematic representation of the batch Sink-Hole Fluidizer; b) Side view of the system before turning on the vibration; and c) Top view of the batch system during an experiment with air and vibration turned on.

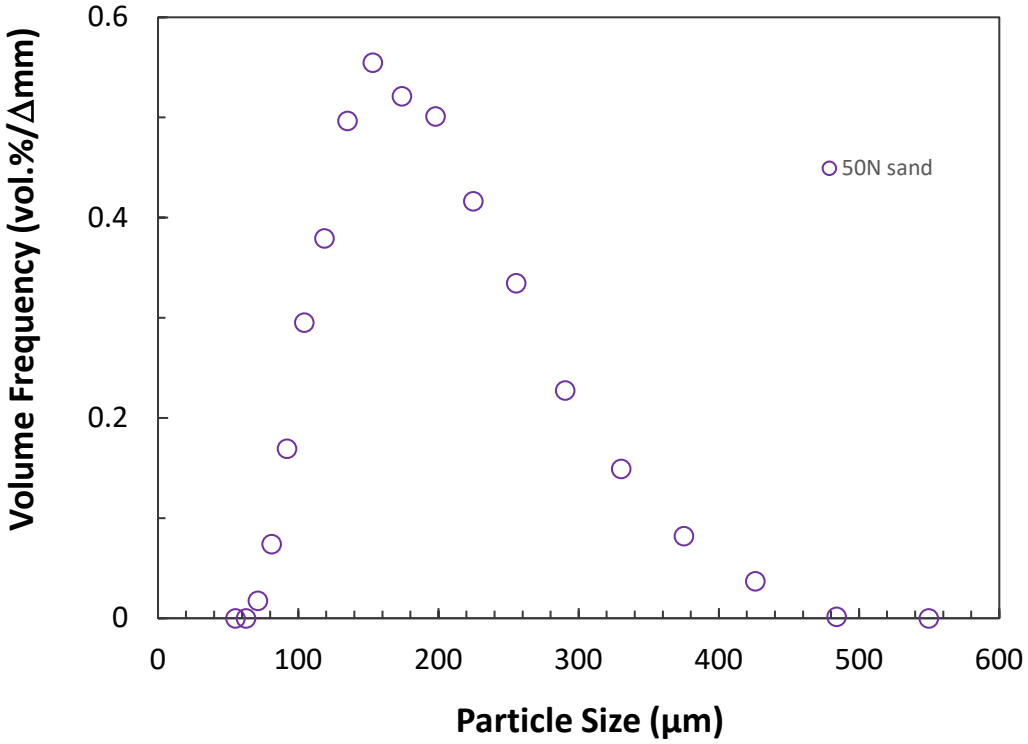

Figure 2: Size distribution of 50N grade sand used as the fluidized media (as measured by Malvern Mastersizer 3000).

3.2 Method

The experimental procedure was similar to that of Kumar et al. (2018). Initially, a given mass of sand media was added to the unit. Then a plug was inserted into the Sink-Hole and coloured tracer particles placed onto the top screen (usually 20 particles of each of the nine density fractions). The air rate was then switched on to the desired level, followed by the vibration. Once the system was running stably, the plug was removed and a timer started. After a given period the plug was re-inserted into the Sink-Hole, the timer stopped and the air and vibration switched off. Once the system had come to rest, the numbers of tracer particles of each density remaining on the upper screen were counted and used to determine the fraction that had partitioned to the underflow. The air and vibration were then switched back on, the plug removed and the timer restarted. This was repeated a number of times. Depending on how quickly the system appeared to reach equilibrium, the number of measurements and the total duration of the experiment varied.

Irregular-shaped tracer particles of 2.0-8.0 mm supplied by Partition Enterprises (Brisbane, Australia) were used to assess the separation performance. The photo in Figure 3 shows a mixture of the nine different density particles from 2400 kg/m^3 to 4800 kg/m^3 with intervals of 300 Δkg/m^3 which could be distinguished based on their colour. They are shown placed on the top screen with the centrally located Sink-Hole; also visible below it is the lower screen used to capture underflow particles. Throughout this paper, the densities are reported using relative density (RD) units, defined as the particle density divided by the density of water (1000 kg/m^3).

The tracer particles were screened to produce four size fractions: 5.6-8.0 mm, 4.0-5.6 mm, 2.8-4.0 mm and 2.0-2.8 mm. For experiments on these individual size fractions, 20 tracers of each of the nine densities were used (so 180 particles total). However, there were no 2.4 RD tracers in the 5.6-8.0 mm size range, so only 160 particles were used in those experiments. Kumar et al. (2018) found that D_{50} and Ep values were fairly stable in the 2.8-8.0 mm size ranges, but increased for 2.0-2.8 mm particles. Therefore, some experiments were performed in this new work using wider 2.8-8.0 mm composite mixtures created by using 10 particles from each of the three coarsest narrow size fractions to give 30 particles in each density interval, with the exception of the 2.4 RD tracer particles which were not available in the 5.6-8.0 mm size range and so had only 20 particles (and thus 260 particles total were used in these composite experiments). This is the reason why the 2.4 RD data is absent in some plots. At each stage/step in the experiment, all the overflow particles were screened and then the number of particles of each size and density fraction counted. The overflow particles were then remixed, replaced on top of the screen and the experiment continued.

Figure 3: Photo of a mixture of the 2.0-8.0 mm tracer particles of nine different densities (distinguished by their colour) placed on the top screen mesh with 60 mm Sink-Hole. The second mesh visible beneath collects the underflow particles and helps suppress bubbling.

The results from each experiment were analyzed to calculate the fraction of particles of each density D reporting to the underflow (the partition P to underflow) as a function of time. At a given instant in time, the method provided the probabilities as a function of the density. Equation 1 (Wills & Finch, 2016) was fitted to each set of partition data by minimising the sum of the error squared between the partition data and the model.

$$P = \frac{1}{1 + \exp[\ \frac{\ln 3(D_{50} - D)}{Ep}]} \qquad (1)$$

The parameter, D_{50}, is referred to as the density cut point, corresponding to the particle with an equal probability of reporting to either the overflow (above the screen) or underflow (below the screen). Similarly, the D_{25} and D_{75} correspond to the particles having a probability of 0.25 and 0.75 respectively of reporting to the underflow, which in this case means they report below the upper screen surface. The Ecart probable, Ep, is defined as half the difference between the D_{75} and D_{25} values, so it is effectively one-quarter of the inverse slope of the partition curve. The uncertainty of

individual partition estimates based on only 20 tracer particles can be calculated using binomial theory, as reported previously (Kumar et al., 2018) using the work of Brown et al. (2001) and Davis and Lyman (1989). There is also significant uncertainty in the D_{50} and Ep values obtained by curve fitting through such partition data spaced at 0.30 RD density intervals. The 95 % confidence intervals of these fitted parameters were estimated using a Monte-Carlo approach, which is explained in more detail in Kumar et al. (2018). The resulting error bars are shown on some plots.

4.0 Results and Discussion

Around 200 experiments were performed in the campaign of work reported in this paper. These experiments all used the same sand media and vibration conditions (Section 3.1). Variations were made to the mass of sand (6.1-6.6 kg), the fluidization air superficial velocity (6.1-7.4cm/s), the size of the Sink-Hole (13-60 mm) and the number and size range of the tracer particles (see Section 3.2). The following sub-sections discuss the effects of Sink-Hole diameter on the separation kinetics and cut size, the effects of tracer particle size, and the effects of air rate. Finally, a speculative mechanism to explain the results is proposed.

4.1 Effect of Sink-Hole Diameter on Separation Kinetics and Density Cut Point

Figures 4a and 4b show typical partition performance as a function of time for 13 mm and 60 mm diameter Sink-Holes respectively. For a 13 mm Sink-Hole, the partition data varied significantly with time, only approaching a stable equilibrium result after around 300 s. In contrast, the 60 mm Sink-Hole had reached a stable equilibrium state within less than 40 s. As found by Kumar et al. (2018), the equilibrium was a dynamic one in which particles that had previously sunk through the Sink-Hole sometimes re-emerged onto the upper screen.

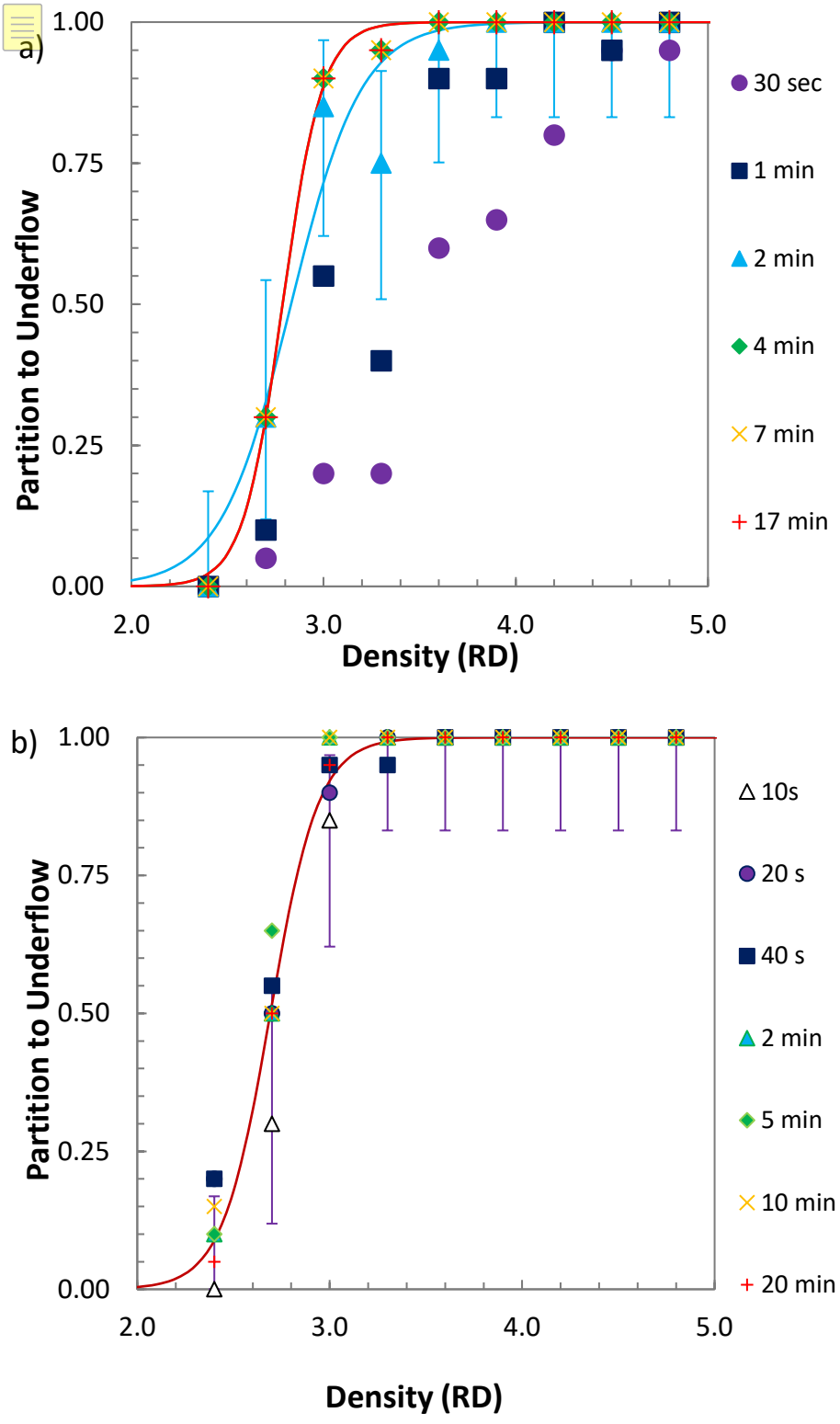

Figure 4: Time based partition data for 4.0-5.6 mm particles with a) a 13 mm diameter Sink-Hole with 6.1 kg bed mass and 6.3 cm/s air rate (the curves show best fits of Equation 1 at t = 2 min and t = 17 min respectively); and b) a 60 mm diameter Sink-Hole with 6.5 kg bed mass and 6.6 cm/s air rate (the curve shows the best fit of Equation 1 through the average of all data). Error bars on t = 2 min partition data in a) and t = 10 s partition data in b) show the 95 % confidence interval obtained by binomial theory for 20 tracer particles.

Figure 5 shows the partition curves at t = 300 s from five experiments with 4.0-5.6 mm tracer particles using different Sink-Hole diameters all at 6.4 kg bed mass and 6.8 cm/s air rate. There is a clear drop in the density cut point as the Sink-Hole diameter increases, but the sharpness of separation remained similar. These trends are more evident in Figure 6 which shows the transient D_{50} and Ep values versus time for different Sink-Hole diameters using 4.0-5.6 mm tracer particles at similar bed masses and air rates. For the smaller 18 mm Sink-Holes, the transient D_{50} values started at around 3.2 RD and gradually dropped, taking more than 5 min (300 s) to approach a stable equilibrium D_{50} value below 3.0 RD. In contrast, the 60 mm diameter Sink-Holes had reached a stable D_{50} value of around 2.65 RD in less than 30 s. The time required to achieve a dynamic steady state clearly reduced steadily with an increase in the diameter of the Sink-Hole. Similar trends were seen for the 2.8-4.0 mm and 5.6-8.0 mm tracer particles across a range of bed mass and air rates. This suggests that the system could achieve a steady state relatively quickly if there were a large number of Sink-Holes of smaller diameter or a small number of Sink-Holes of larger diameter. Larger Sink-Holes would also offer the ability to separate particles of a larger size.

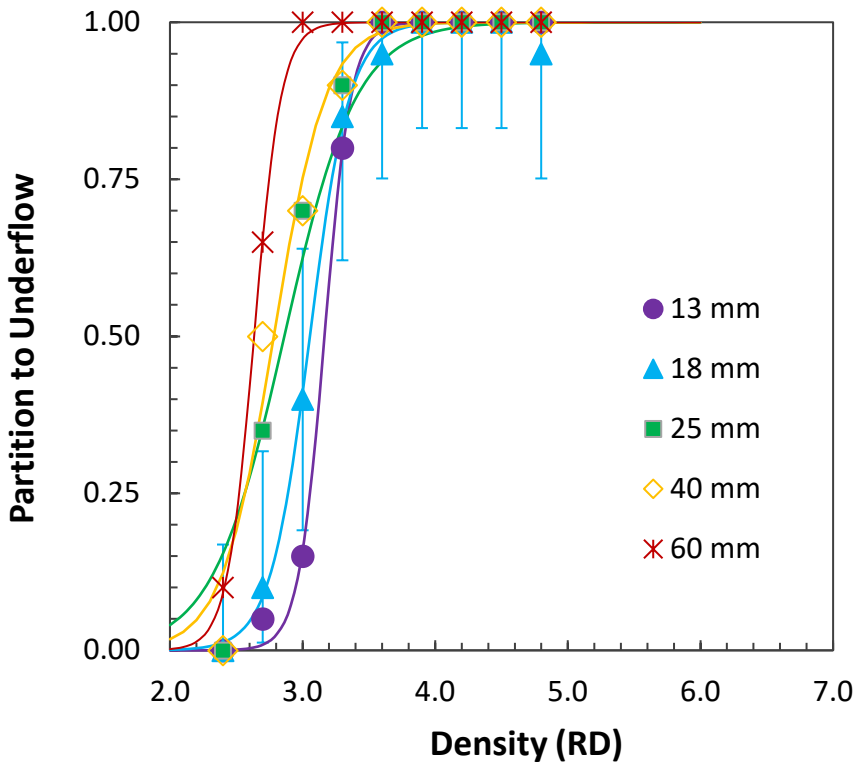

Figure 5: Partition performance after 300 s for 4.0-5.6 mm particles with different Sink-Hole sizes under the same operating conditions (6.4 kg bed mass and 6.8 cm/s air rate). Error bars on 18 mm partition data shows the 95 % confidence interval obtained by binomial theory.

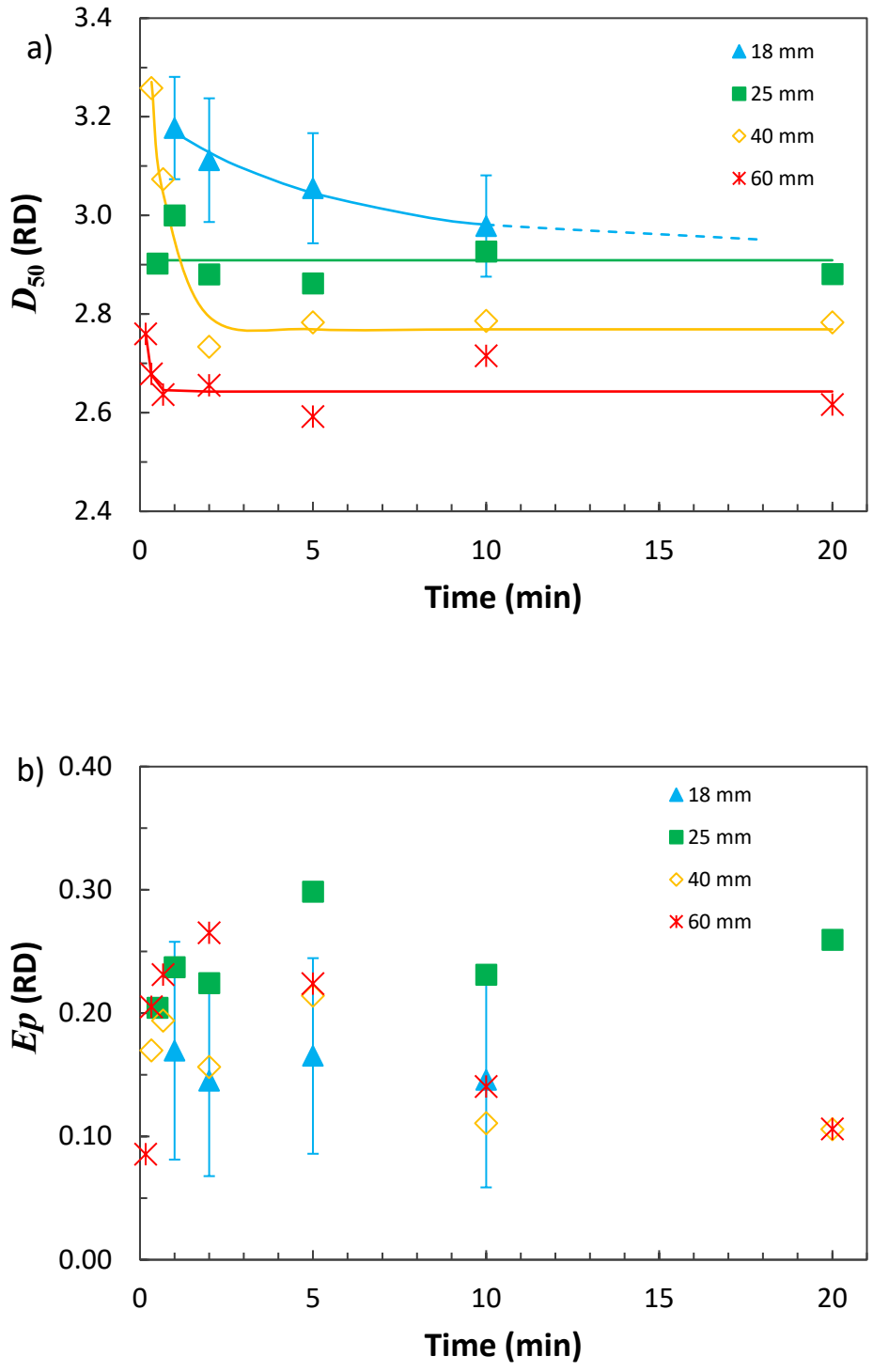

Figure 6: Transient a) D_{50}, and b) Ep values of experiments performed with different Sink-Hole diameters for 4.0-5.6 mm tracer particles under similar operating conditions of around 6.4 kg bed mass and 6.8 cm/s air rate (exact values shown in Appendix 1). Vertical error bars on 18 mm Sink-Hole indicate the 95 % confidence interval generated through Monte-Carlo simulations. Lines in Figure (a) show the best fits of Equation (2) through the data (Table 2).

To objectively quantify the equilibrium separation density $D_{50,e}$ and the kinetics of approaching equilibrium, an exponential decay model with three-parameters (Equation 2) was fitted through the transient D_{50} data by minimising the sum of squared error.

$$D_{50}(t) = D_{50,e} + \left(D_{50,0} - D_{50,e}\right)\exp(-kt) \qquad (2)$$

The fitted parameter k is the rate constant for approaching the equilibrium value $D_{50,e}$. The $D_{50,0}$ value nominally indicates the transient cut point density at the start of the experiment when t = 0. However, this value is indefinite since all the particles start on the top, so it is essentially just a parameter that floats to give the best fit through the data, with the constraint that $D_{50,0} \geq D_{50,e}$. Table 2 shows these fitted values for the experimental data shown in Figure 6a. These provide objective support for the decrease in $D_{50,e}$ values and increase in kinetic k values with increasing Sink-Hole size. The trend of decreasing D_{50} with increasing Sink-Hole size is unsurprising. Presumably increasing the Sink-Hole diameter further must eventually lead to a situation where the mechanism that generates the high cut points break down, and the separation density becomes the same as that of a conventional fluidized bed i.e. equal to the average density of the fluidized bed.

Table 2: Least square error best fits values of k, $D_{50,e}$ and $D_{50,0}$ to transient partition data in Figure 6a. Note that the k value is undefined for the 25 mm data since $D_{50,e}$ = $D_{50,0}$ in this case.

Sink-Hole (mm)	18	25	40	60
$D_{50,e}$	2.94	2.91	2.77	2.64
$D_{50,0}$	3.22	2.91	3.68	3.05
k	0.20	ND	1.79	7.50

The transient Ep values remained fairly stable during all the experiments as shown in Figure 6b. Again, similar trends were seen for the 2.8-4.0 mm and 5.6-8.0 mm tracer particles across a wide range of operating conditions. Typical Ep values were of order 0.2 – 0.3 RD, which when divided by the separation density gave imperfection (Ep/D_{50}) values below 0.10. This sharpness of separation is in the range described qualitatively as representing “excellent” separation performance (Murthy & Basavaraj, 2012).

4.2 Effect of Air Rate and Bed Mass

As reported previously (Kumar et al., 2018), for a given Sink-Hole diameter the separation density could also be varied by changing the air rate or bed mass. The same general trends were seen in this work with larger Sink-Hole diameters. For instance Figures 7a and 7b show the effect of a change in the air velocity on the fitted D_{50} and Ep values respectively for various Sink-Hole diameters and

tracer particle size ranges, all at a constant bed mass of 6.5 kg. At low air rates, such as 6.1 cm/s, there was insufficient bed expansion, hence the granular media failed to reach the level of the Sink-Hole, producing a very low separation density of about 1.75 RD (close to the fluidized bed bulk density estimated to be around 1.8 RD), and a very poor Ep of about 0.73 RD. At higher air rates, the bed expansion forced the granular media up through the Sink-Hole, resulting in much higher separation densities. The D_{50} values then steadily decreased with increasing air rate (as seen also in Kumar et al. (2018)). The Ep values remained fairly stable for air velocities from 6.3 to 6.8 cm/s. Similar trends were seen for a wide range of bed masses and Sink-Hole sizes. At air velocities greater than 6.8 cm/s with the larger 60 mm Sink-Holes, the cut point density had dropped below 2.4 RD and so was no longer able to be accurately measured using the tracer particles available in this study (*cf*. the large uncertainty of the D_{50} = 1.75 RD value at 6.1 cm/s air rate). As noted by Kumar et al. (2018), a gradual drop in density cut point with increasing air rate is what would also be expected in a conventional fluidized bed, where bed expansion would cause a drop in bed bulk density. However, here the cut points are much higher than the bed bulk density, indicating that some other separation mechanism is also at play.

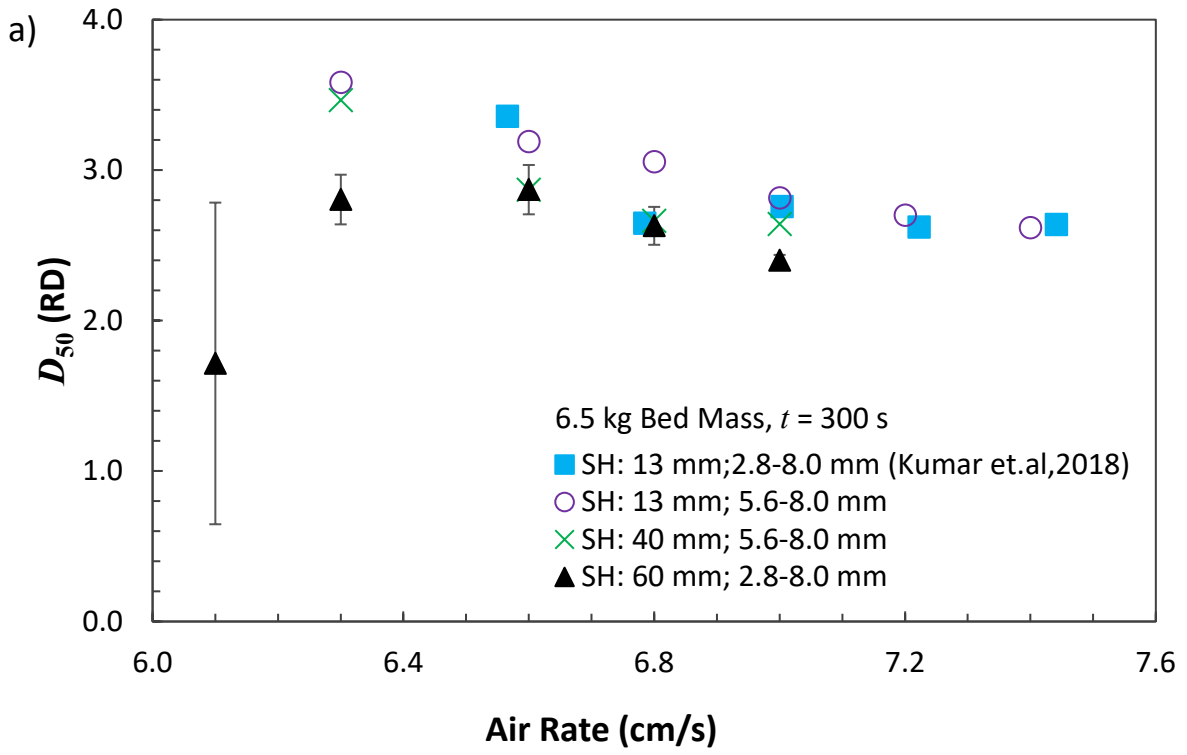

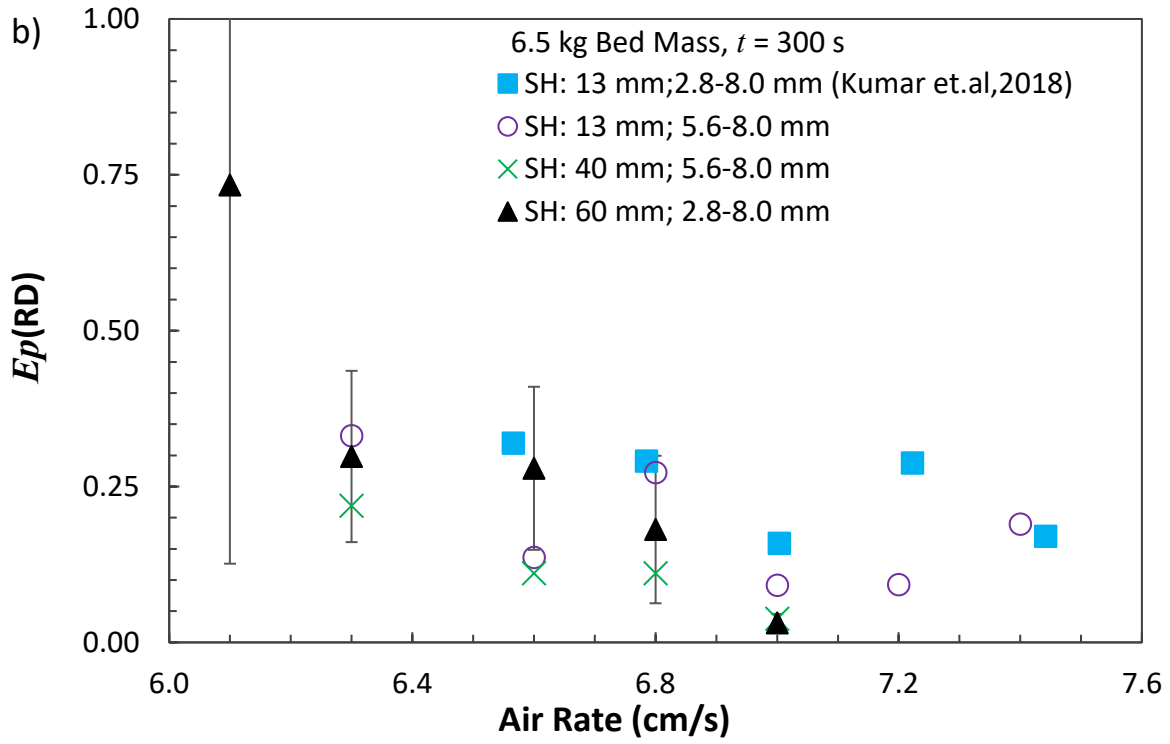

Figure 7: (a) D_{50} and (b) *Ep* behaviour versus air rate after 300 s with 6.5 kg bed mass. Sink-Hole (SH) diameter and range of tracer particle sizes indicated in the legend. Vertical error bars on 60 mm Sink-Hole indicate the 95 % confidence interval generated through Monte-Carlo simulations.

4.3 Impact of Particle Size on Separation Density

It was reported previously that there was a significant increase in the separation density with decreasing particle size when going below 2.8 mm size, but that above 2.8 mm in size performance was fairly stable up to 8.0 mm (Kumar et.al, 2018). Figure 8 plots data from the appendices of Kumar et al. (2018) together with additional new data for 2.0-2.8 mm particles. For most operating conditions, the variation in separation densities of the 2.8-4.0, 4.0-5.6 and 5.6-8.0 mm size ranges was well within the 95 % confidence interval generated through Monte-Carlo simulations (Figure 8). Again, these separation densities were higher than the medium bulk density and across all the work in over 90 % of cases were higher even than the skeletal media density of 2.6 RD.

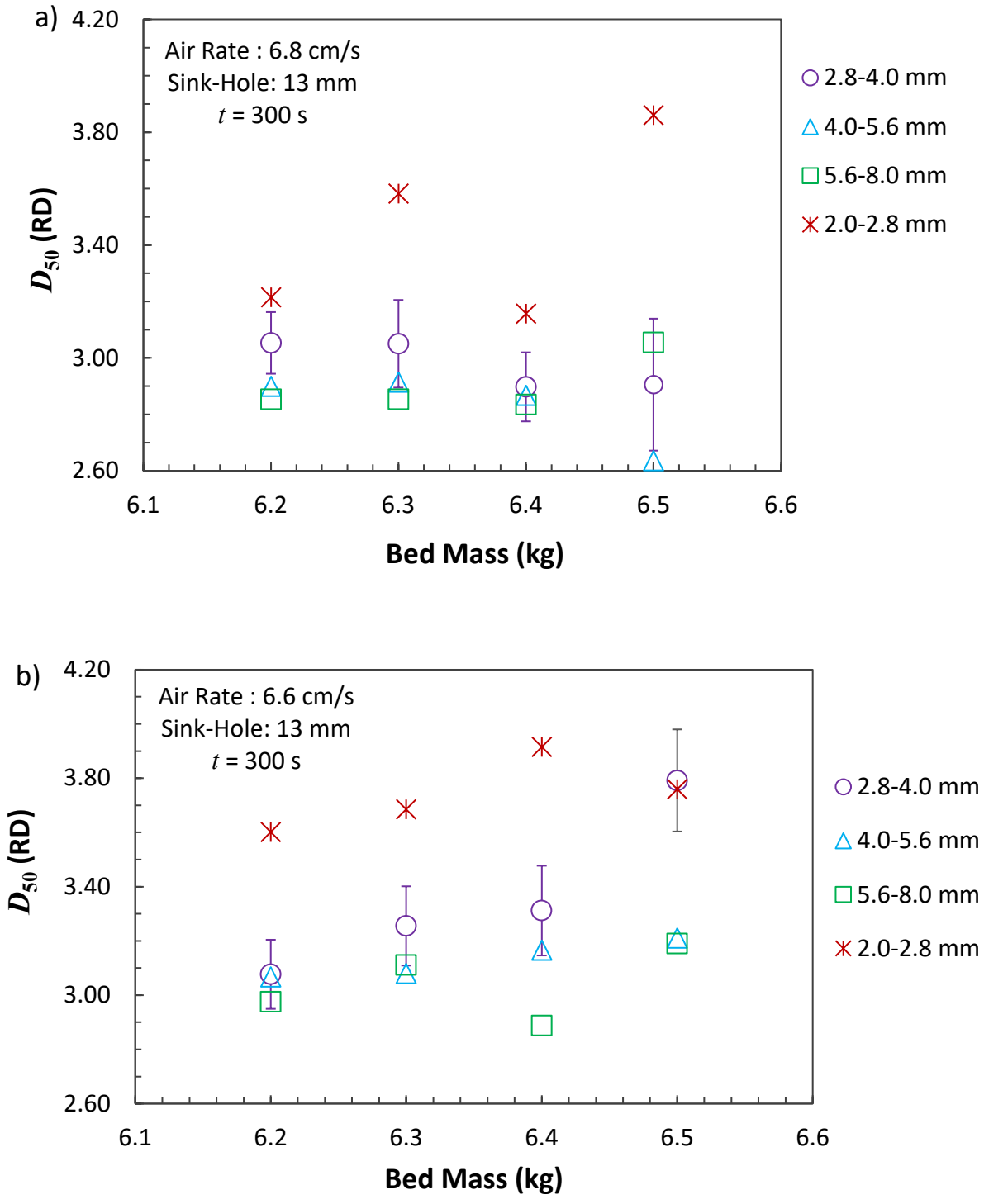

Figure 8: Separation densities achieved with experiments performed using 13 mm Sink-Hole with the four narrow size ranges of particles between 2.0-8.0 mm with air rate varying bed mass and superficial air velocities of (a) 6.8 cm/s and (b) 6.6 cm/s. Vertical error bars on 2.8-4.0 mm data indicate the 95 % confidence interval generated through Monte-Carlo simulations.

Some experiments were also performed using a 2.8-8.0 mm composite feed consisting of 10 particles in each of the 2.8-4.0, 4.0-5.6 and 5.6-8.0 mm size intervals, for each of the nine density

fractions. There were no 2.4 RD particles in the 5.6-8.0 mm size range, so this gave a total of 260 tracer particles, compared to the 160 or 180 particles in a standard experiment with a narrow particle size range. Figure 9 shows the transient D_{50} and Ep values of the narrow and broad size range for the 25 mm diameter Sink-Hole with a bed mass of 6.25 kg and air rate of 7.0 cm/s. Hence even though the narrow size fraction data are here based on only 10 particles in each density interval and thus would be expected to show considerable scatter, the narrow size fraction D_{50} and Ep results were not significantly different to the composite data. Thus again the separation cut point is shown to be relatively insensitive to particle size in this size range.

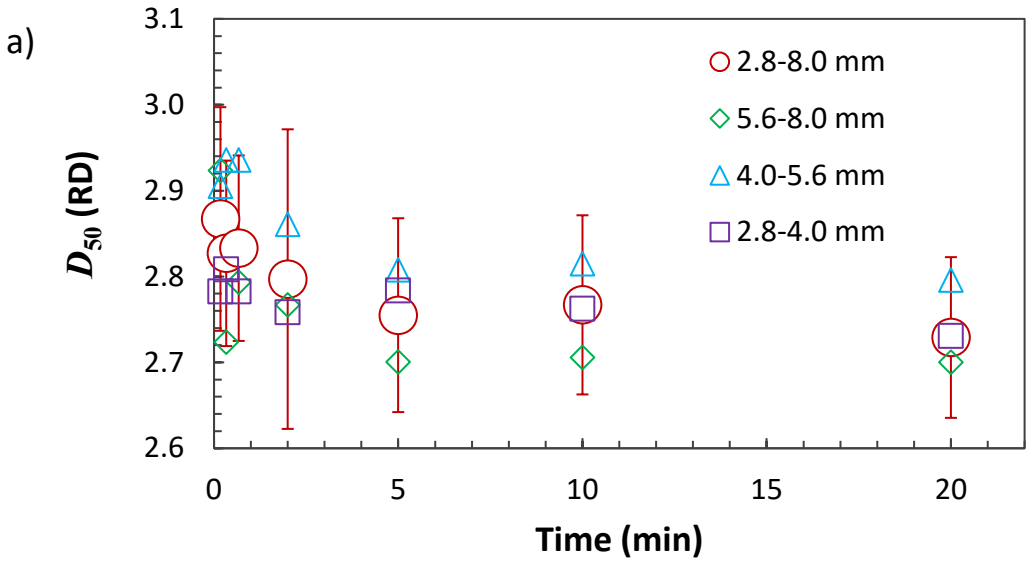

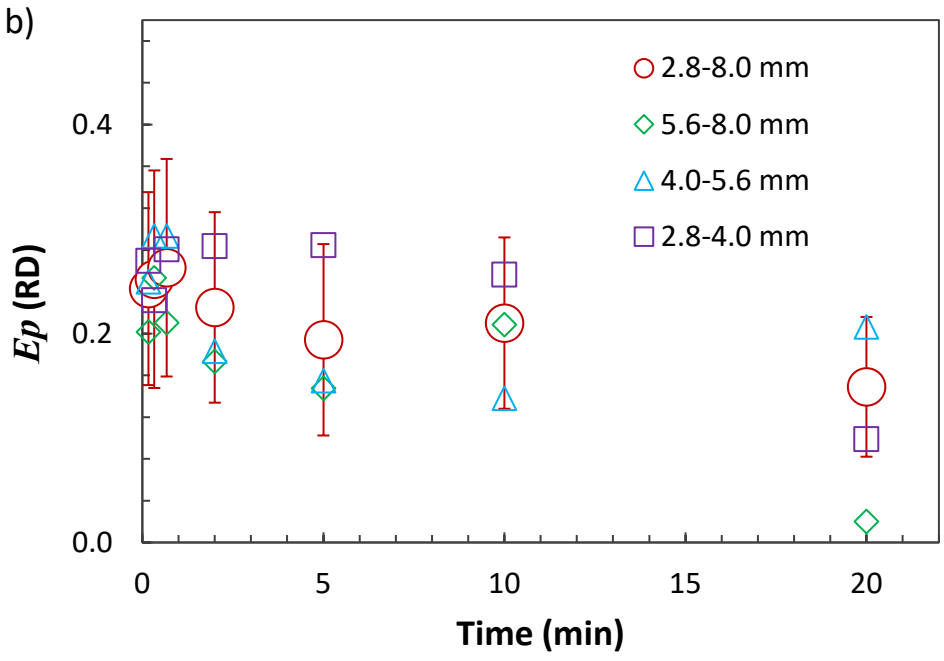

Figure 9: Transient (a) D_{50} and (b) Ep results for narrow size fractions during an experiment performed with a composite feed (2.8-8.0 mm) with a 25 mm Sink-Hole, 6.25 kg bed mass and 7.0 cm/s air rate. The results suggest that the D_{50} and Ep values found using narrow size ranges were within the 95 % confidence interval of the composite values. Raw data are in Appendix 2. Vertical error bars on the composite results show the 95 % confidence interval generated by Monte-Carlo simulations based on 30 particles (Kumar et al., 2018).

4.4 Speculative Jamming Mechanism

This work has confirmed the previous findings of Kumar et al. (2018) that the Sink-Hole separation density was significantly higher than the approximate 1800 kg/m^3 bulk density of the fluidized bed formed by silica sand with the skeletal density of 2600 kg/m^3 and air. Remarkably, sometimes separation densities greater than 3000 kg/m^3 were obtained, much higher even than the density of the silica media (Figures 6, 7, and 8). This means that the mechanism responsible for the separation is not governed by the principle of buoyancy in a dense medium, but by some other granular mechanism.

A glass transition condition could yield a solid-like state capable of supporting particles of almost any density. But the evidence from the experiments supports the view that the medium continued to exhibit liquid-like properties given that a particle of marginally higher density would tend to sink, and particles of much higher density would easily sink. This means that the state of the system bridges the extremes of the solid-like and liquid-like binary states. The novel granular arrangement appears to expand the transition between these extremes, all within a relatively thin, two-dimensional layer near the mouth of the Sink-Hole.

It is postulated that the tracer particle produces a local deformation of the granular state. Presumably, the deformation produced by an 8 mm diameter particle must be far stronger than that produced by a 2.8 mm diameter particle. However, particles of both sizes separate through the media at almost the same density. This means the granular state involves a macro-structure that is size invariant.

We are reminded of the self-organised critical states that develop naturally by interacting dynamical systems, driven by external energy sources (Bak et al., 1987). The favourable flow of the granular medium upwards through the so-called Sink-Hole provides the precursor for jamming, a consequence of solid-solid contacting, and local de-fluidization, or filtration of air from the medium. It is postulated that temporal interlocking of the particles across the Sink-Hole, coupled with the deformation caused by the large particles in the Sink-Hole, conspire to support the weight of the particle. The state is critical, with a small increase in the weight per unit volume of the large tracer

particle being enough to break through these connections. Further investigation is required to better understand the mechanism and determine if this postulate is correct.

5.0 Conclusions

The processing time for achieving a complete density-based separation decreased as the diameter of the Sink-Hole increased, achieving steady state in less than 30 s for a 60 mm diameter hole compared to over 5 min for a 13 mm Sink-Hole. Increasing the Sink-Hole diameter lowered the separation density under the same operating condition. Increasing the air rate gradually lowered the separation density. The observed sharp partition curves with low imperfection values (< 0.1) indicate that the separation device is efficient and robust, while offering the potential to separate at higher bed densities. Remarkably the separation density was found to be higher than the medium bulk density, and in many cases higher even than the skeletal density of the granular media. Moreover, the separation density was virtually independent of the tracer particle size in the range of 2.8 to 8.0 mm. The observed phenomenon was attributed to a jamming mechanism, but further investigation is required to confirm this postulate.

6.0 Acknowledgements

The authors gratefully acknowledge the Australian Research Council Research Hub for Advanced Technologies for Australian Iron Ore (Grant Number: IH130200031) and our industry partners for their financial support.

7.0 References

Bak, P., Tang, C., & Wiesenfeld, K. (1987). Self-organized criticality: An explanation of the 1/f noise. *Physical Review Letters, 59*(4), 381-384. doi:10.1103/PhysRevLett.59.381

Batchelor, G. K. (1982). Sedimentation in a dilute polydisperse system of interacting spheres. Part 1. General theory. Journal of Fluid Mechanics, 119, 379-408. doi:10.1017/S0022112082001402

Beeckmans, J. M., & Macwilliam, K. (1986). Stabilization of a fluidized bed by horizontal vibrations. *Powder Technology, 45*(2), 177-181. doi:http://dx.doi.org/10.1016/0032-5910(66)80011-6

Brown, L. D., Cai, T. T., & DasGupta, A. (2001). Interval Estimation for a Binomial Proportion. *Statist. Sci., 16*(2), 101-133. doi:10.1214/ss/1009213286

Clift, R., Seville, J. P. K., Moore, S. C., & Chavarie, C. (1987). Comments on buoyancy in fluidized beds. *Chemical Engineering Science*, 42(1), 191-194. doi:https://doi.org/10.1016/0009-2509(87)80228-2

Davis, J. J., & Lyman, G. J. (1989). A Numerical Study of the Effect of Density Tracer Numbers and Properties on the Accuracy of Calculated Partition Data. *Coal Preparation, 7*(3-4), 199-210. doi:10.1080/15455838909407966

Dwari, R. K., & Rao, K. H. (2007). DRY BENEFICIATION OF COAL—A REVIEW. *Mineral Processing and Extractive Metallurgy Review, 28(3)*, 177-234. doi:10.1080/08827500601141271

Geldart, D. (1973). Types of gas fluidization. *Powder Technology, 7*(5), 285-292. doi:http://dx.doi.org/10.1016/0032-5910(73)80037-3

Gidaspow, D. (1994). Gidaspow (Ed.), *Multiphase Flow and Fluidization*. San Diego: Academic Press.

Kumar, D., Iveson, S. M., & Galvin, K. P. (2018). Dry separation using a fluidized Sink-Hole. *Minerals Engineering, 127*, 105-113. doi:https://doi.org/10.1016/j.mineng.2018.07.021

Kunii, D., & Levenspiel, O. (1991). *Fluidization Engineering (Second Edition)*. Boston: Butterworth-Heinemann.

Luo, Z., Fan, M., Zhao, Y., Tao, X., Chen, Q., & Chen, Z. (2008). Density-dependent separation of dry fine coal in a vibrated fluidized bed. *Powder Technology, 187*(2), 119-123. doi:http://dx.doi.org/10.1016/j.powtec.2008.02.001

Marring, E., Hoffmann, A. C., & Janssen, L. P. B. M. (1994). The effect of vibration on the fluidization behaviour of some cohesive powders. *Powder Technology, 79*(1), 1-10. doi:http://dx.doi.org/10.1016/0032-5910(94)02810-9

Mawatari, Y., Koide, T., Tatemoto, Y., Takeshita, T., & Noda, K. (2001). Comparison of three vibrational modes (twist, vertical and horizontal) for fluidization of fine particles. *Advanced Powder Technology, 12*(2), 157-168. doi:http://dx.doi.org/10.1163/15685520052384998

Mori, S. (1990). Vibro-Fluidization of Group-C Particles and its Industrial Application. *AIChE Symp. Ser., 86*(276), 88-94.

Murthy, N., & Basavaraj, K. (2012). Assessing the performance of a floatex density separator for the recovery of iron from low-grade australian iron ore fines− a case study. *Paper presented at the XXVI International Mineral Processing Congress (IMPC).*

Oshitani, J., Franks, G. V., & Griffin, M. (2010). Dry dense medium separation of iron ore using a gas–solid fluidized bed. *Advanced Powder Technology, 21*(5), 573-577. doi:http://dx.doi.org/10.1016/j.apt.2010.02.014

Oshitani, J., Kawahito, T., Yoshida, M., Gotoh, K., & Franks, G. V. (2011). The influence of the density of a gas–solid fluidized bed on the dry dense medium separation of lump iron ore. *Minerals Engineering, 24*(1), 70-76. doi:http://dx.doi.org/10.1016/j.mineng.2010.10.010

Oshitani, J., Kajimoto, S., Yoshida, M., Franks, G. V., Kubo, Y., & Nakatsukasa, S. (2013). Continuous float–sink density separation of lump iron ore using a dry sand fluidized bed dense medium. *Advanced Powder Technology, 24*(2), 468-472. doi:https://doi.org/10.1016/j.apt.2012.10.010

Patil, D. P., & Parekh, B. K. (2011). Beneficiation of Fine Coal Using the Air Table. *International Journal of Coal Preparation & Utilization, 31(3/4),* 203-222. doi:10.1080/19392699.2011.574948

Rhodes, M. J., & Rhodes, M. (2008). *Introduction to particle technology*: John Wiley & Sons.

Wills, B. A., & Finch, J. A. (2016). *Wills' mineral processing technology: an introduction to the practical aspects of ore treatment and mineral recovery.*

Appendix 1: Bed mass and air rates used for experiments shown in Figure 6. All data is for 4.0-5.6 mm tracer particles after t = 300 s.

Sink-Hole (mm)	13	18	25	40	60
Bed Mass (kg)	6.4	6.4	6.4	6.45	6.5
Air Rate (cm/s)	6.8	6.8	6.8	6.8	6.6

Appendix 2: Raw data for experiments reported in Figure 9.

	5.6-8.0 mm		**4.0-5.6 mm**		**2.8-4.0 mm**		**Composite 2.8-8.0 mm**			
Time (min)	D_{50}	Ep	D_{50}	D_{50}	Ep	Ep	D_{50}	Ep	D_{50} 95% confidence interval	Ep 95% confidence interval
0.17	2.92	0.20	2.91	2.87	0.24	0.25	2.78	0.27	0.13	0.09
0.33	2.72	0.25	2.94	2.83	0.25	0.29	2.81	0.23	0.11	0.10
0.67	2.79	0.21	2.94	2.83	0.26	0.29	2.78	0.28	0.11	0.10
2	2.77	0.17	2.86	2.80	0.23	0.18	2.76	0.28	0.17	0.09
5	2.70	0.15	2.81	2.76	0.19	0.15	2.78	0.28	0.11	0.09
10	2.71	0.21	2.81	2.77	0.21	0.14	2.76	0.26	0.10	0.08
20	2.70	0.02	2.80	2.73	0.15	0.21	2.73	0.10	0.09	0.07